Quantitative Coherent Anti-Stokes Raman Scattering (CARS) Microscopy

7 AUTHORS, INCLUDING:

Katrin F. Domke

Max Planck Institute for Polymer Research

30 PUBLICATIONS **840** CITATIONS

SEE PROFILE

Hideaki Kano

The University of Tokyo

64 PUBLICATIONS **1,026** CITATIONS

SEE PROFILE

Erik Vartiainen

Lappeenranta University of Technology

70 PUBLICATIONS **985** CITATIONS

SEE PROFILE

Mischa Bonn

Max Planck Institute for Polymer Research

347 PUBLICATIONS **7,569** CITATIONS

SEE PROFILE

# Quantitative Coherent Anti-Stokes Raman Scattering (CARS) Microscopy

James P. R. Day,[†] Katrin F. Domke,[†] Gianluca Rago,[†] Hideaki Kano,[‡] Hiro-o Hamaguchi,[‡] Erik M. Vartiainen,[§] and Mischa Bonn*[,†]

[†]FOM Institute for Atomic and Molecular Physics (AMOLF), Science Park 104, 1098 XG, Amsterdam, The Netherlands
[‡]Department of Chemistry, School of Science, The University of Tokyo, Hongo 7-3-1 Bunkyo-ku Tokyo, 113-0033, Japan
[§]Department of Mathematics and Physics, Lappeenranta University of Technology, B. O. Box 20, FI-53851, Lappeenranta, Finland

ABSTRACT: The ability to observe samples qualitatively at the microscopic scale has greatly enhanced our understanding of the physical and biological world throughout the 400 year history of microscopic imaging, but there are relatively few techniques that can truly claim the ability to quantify the local concentration and composition of a sample. We review coherent anti-Stokes Raman scattering (CARS) as a quantitative, chemically specific, and label-free microscopy. We discuss the complicating influence of the nonresonant response on the CARS signal and the various experimental and mathematical approaches that can be adopted to extract quantitative information from CARS. We also review the uses to which CARS has been employed as a quantitative microscopy to solve challenges in material and biological science.
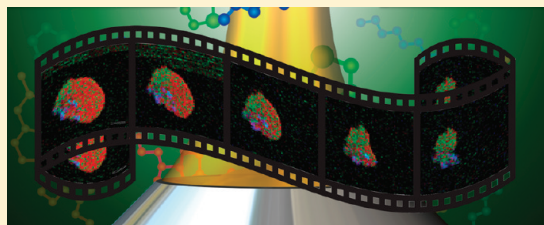
INTRODUCTION

The history of microscopic imaging dates back 400 years to the time of Galileo, and since that time, a substantial range of techniques has been developed to allow researchers to observe microscopic features within biological or inorganic samples. The contrast in these imaging techniques can arise from many different physical responses. For example, in the case of bright-field imaging, the varying intensities within an image are caused by differences in the absorption or scattering of the incident white light. While these differences do originate from variations in the spatial distribution of different molecules in the sample, generally, most microscopic techniques are unable to report more than the qualitative variation in the sample composition. Many questions in biological and materials science however require one to go beyond a qualitative observation of a microscopic sample. For example, one may wish to know the local concentration of a particular molecule, such as a drug, within a cell in order to follow its uptake and metabolism. As another example, one may be interested in the composition of reagents and products within a heterogeneous catalyst crystal during the catalytic conversion process in order to determine reaction pathways and rates and the spatial distribution of reactive sites within the catalyst crystal. To observe such processes in a truly quantitative manner, a microscopic imaging technique should fulfill the following two criteria: it should distinguish precisely between different chemical species (preferably without the need for exogenous labels) and it should quantify the local concentrations of those species on the microscopic scale. In this contribution, we show that coherent anti-Stokes Raman scattering (CARS) microscopy realizes both of these requirements, and we review its use as a quantitative microscopic imaging technique.

There are a number of other quantitative probes that can be used as microscopic imaging techniques.[1] In confocal fluorescence microscopy, a specimen is labeled with a fluorescent dye molecule (fluorophore). Confocal fluorescence microscopy is highly sensitive, and several experimental geometries have been developed that extend the spatial resolution far beyond the diffraction limit; for example, with stimulated emission depletion (STED), a spatial resolution better than 10 nm can be achieved.[2] However, unless the sample is autofluorescent, fluorescence microscopy is not a label-free technique, and only the tagged constituents of a sample are observed. On the one hand, the use of site-specific labels is beneficial as it simplifies the interpretation of otherwise complex microscopic images, but on the other hand, the introduction of fluorophores can affect the native behavior of the sample. The fluorescence intensity is linear in concentration at low concentrations,[3] but the fluorophore may be degraded by (photo)-chemical reactions that cause photobleaching. Fluorophores can also suffer from fluctuations in the emitted intensity in a process known as blinking. These factors all affect the quality of the quantitative response.

X-ray fluorescence microscopy (μXRF) involves the detection of secondary X-rays from a sample that has been illuminated by an intense primary X-ray source. μXRF is quantitatively sensitive to inorganic species (particularly metals) at concentrations down to 0.1 ppm and can probe the elemental makeup of the sample with submicrometer resolution.[4] However, this approach requires cryogenic preparation of the sample and synchrotron radiation to achieve the highest sensitivity.

Imaging mass spectrometry (IMS) employs a focused probe beam to bombard a sample in ultrahigh vacuum.[5] Ion fragments are emitted from the surface of the sample and detected by a mass spectrometer. The most common types of probe beams consist of ions and photons, used in secondary ion MS (SIMS) and matrix-assisted laser desorption/ionization (MALDI), respectively. The surface of the sample is gradually ablated by the ion beam to generate a 3D image. MALDI is capable of lateral resolution in the micrometer range, whereas SIMS can achieve 3D resolution down to some tens of nanometers. IMS is label-free and can readily distinguish different species within a sample (down to nM concentrations in the case of MALDI). Although MS is quantitative, in practice, ion suppression effects, in which the local environment ionizes more readily than the analyte of interest, can complicate significantly the interpretation of quantitative data, particularly in biological tissue.[6] IMS also requires extensive sample preparation including sectioning, cryo-fixation, and matrix deposition and is inherently invasive and necessarily destructive.

There are several types of microscopic imaging techniques that are based on vibrational contrast. All molecules inherently possess vibrations, and the different functional groups within a molecule vibrate at different frequencies. These two factors make molecular vibrations a highly useful contrast agent; these imaging techniques are label-free, chemically specific, and potentially quantitative. Infrared (IR) microscopy is sensitive to the absorption of IR light by a sample. Although IR microscopy fulfills both criteria for a quantitative microscopy, the spatial resolution is limited to $2.5-25$ μm, owing to the long wavelength of IR light. Furthermore, IR is strongly absorbed by water, which can limit the application of IR microscopy, particularly in bioimaging, although the greater brightness available from synchrotron IR radiation extends significantly the potential of IR microscopy.[7]

Spontaneous Raman scattering is an alternative type of vibrational microscopy that circumvents some of the limitations of IR microscopy.[1] It is an inelastic scattering technique that employs visible or near-IR light as the excitation source. Consequently, the lateral and depth resolutions are considerably better than those in IR microscopy (down to 250 nm and 1 μm, respectively, for a confocal setup). Also, the Raman scattering cross section of water is relatively low compared to organic molecules, which means that this imaging technique is readily applicable to bioimaging. However, the spontaneous Raman process is relatively weak (only $\sim10^{-7}$ of the incident photons are inelastically scattered), which can result in long acquisition times for high-quality images obtained using spontaneous Raman. Furthermore, the spontaneous Raman signal is often dwarfed by single-photon fluorescence. As will be shown later in this article, coherent Raman techniques such as CARS and stimulated Raman scattering (SRS) circumvent some of the intrinsic limitations of (incoherent) spontaneous Raman scattering and thus appear to offer a very appealing approach to label-free quantitative microscopy based on molecular vibrations.

Indeed, CARS microscopy has matured rapidly since its development into a viable technique by the Xie group in 1999,[8] following pioneering work by Duncan in the early 1980s.[9] It is now routinely used to study problems across a range of scientific disciplines, including cell and tissue biology,[10−13] cytometry,[14] catalysis,[15] and reaction kinetics.[16] The contrast in CARS images is derived from the unique vibrational fingerprints shown by different molecules. This sensitivity to molecular vibrations enables CARS microscopy to fulfill the first of the two criteria; CARS is chemically specific without the need for exogenous labeling.

Often, this vibrational contrast alone is sufficient to report on, for example, lipid storage and metabolism within a living cell[10] or the morphology of biological tissue for cancer screening.[17] Indeed, this use of CARS purely as a label-free, chemically specific bioimaging technique for lipids is the most prevalent in the literature. However, CARS microscopy also fulfills the second criterion; the signal is dependent on the concentration of chemical species. Unfortunately, this concentration information is generally not immediately accessible from the raw CARS signal, which has limited the extent to which CARS microscopy has been used as a fully quantitative imaging technique. Nevertheless, in recent years, a number of schemes have been developed to allow researchers to access this quantitative information, and we review here these approaches and the questions to which they have been applied.

There are two complementary approaches to CARS microscopy, single-frequency CARS and multiplex CARS. In single-frequency CARS, one addresses an individual vibrational resonance (such as the methylene symmetric stretching mode of lipids at ~2845 cm^{-1}), and the CARS response at that frequency is imaged across the sample. This approach allows the rapid acquisition of images (at rates up to 30 frames s^{-1}).[18] Single-frequency CARS is most suitable when images are sought that exhibit qualitative contrast based on vibrational differences in the sample, but the lack of spectral information limits its applicability as a quantitative imaging technique. In multiplex CARS, one addresses a broad range of vibrational resonances simultaneously. Imaging is accordingly slower than single-frequency CARS, but more spectral information is acquired at each location within the sample, which makes the extraction of quantitative information considerably simpler than that for single-frequency CARS microscopy.

Multiplex CARS microscopy is comparable to spontaneous Raman microscopy; in both techniques, a vibrational spectrum is acquired at each location in the image (hyperspectral imaging). However, the nonlinear and coherent nature of CARS results in a signal enhancement of typically several orders of magnitude compared to that of Raman. Here, it should be noted that the CARS signal depends on the incident laser intensity in a nonlinear fashion, whereas in spontaneous Raman, a simple linear scaling applies. Hence, for samples that are susceptible to photodamage, spontaneous Raman microscopy may in some cases be more appropriate.[19] In addition to the generally higher sensitivity of CARS, its spatial resolution is superior to spontaneous Raman, owing to the cubic dependency on the incident laser intensity, and it is intrinsically confocal and directional. Thus, while in spontaneous Raman scattering Stokes light originating from elsewhere in the sample may be scattered into the confocal volume, this complication is largely eliminated in CARS. Also, the CARS signal is blue-shifted relative to the incident beams; therefore, single-photon fluorescence does not degrade the signal. Generally, much shorter acquisition times are required in multiplex CARS experiments than in spontaneous Raman experiments to achieve a comparable signal-to-noise ratio.

SRS is an alternative form of coherent vibrational Raman spectroscopy to CARS where there is no nonresonant term at the detection frequency (vide infra), and hence, the response is linear in concentration. The stimulated Raman signal manifests as a small intensity variation of the incident beams, either as a stimulated Raman loss of the pump beam or a stimulated Raman gain of the Stokes beam. There are two approaches to detect this variation in laser intensity, which is typically on the order of 10^{-4} or less. In SRS microscopy, narrow-band laser sources are coupled to
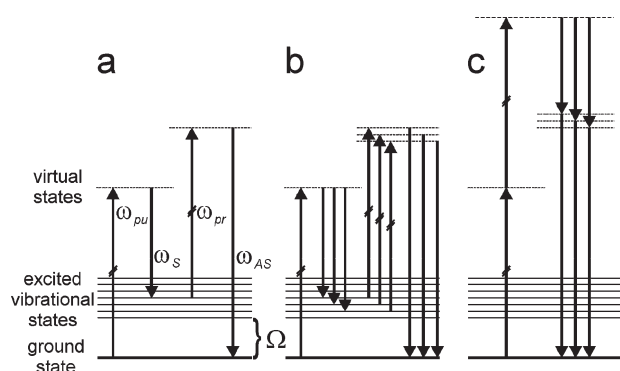
Figure 1. CARS energy level diagrams: (a) vibrationally resonant scheme for single-frequency CARS, (b) vibrationally resonant scheme for multiplex CARS, and (c) a nonresonant scheme. ω_{pu}, ω_S, ω_{pr}, and ω_{AS} are the pump, Stokes, probe, and anti-Stokes frequencies, respectively, and Ω is the frequency of a vibrational mode. For the schemes shown here, $\omega_{pu} = \omega_{pr}$, as indicated by the two short diagonal lines dissecting the pump and probe arrows. The nonresonant transitions do not probe the vibrational energy levels.

lock-in detection to detect intensity variations in the laser beams as low as 10^{-7}.[20,21] However, lock-in detection is not suited to multiplexing, and therefore, SRS microscopy suffers from the same restrictions as single-frequency CARS imaging for quantitative analysis of complex samples with overlapping vibrational resonances. In femtosecond stimulated Raman microscopy developed by Gilch and co-workers, the Stokes pulse is spectrally broad, and the detection is multiplexed.[22,23] However, without lock-in detection, the sensitivity is much reduced, and this approach has not yet been applied to biological samples nor to quantitative measurements of dilute species. Moreover, although in SRS there is no nonresonant term at the detection frequency, other nonlinear optical processes such as cross-phase modulation and ground-state depletion can degrade the vibrational contrast.[24] In this Feature Article, we will limit ourselves to a discussion of quantitative CARS while acknowledging the potential of stimulated Raman as a quantitative technique.

■ RETRIEVING QUANTITATIVE INFORMATION FROM CARS MICROSCOPY

In this section, we describe the CARS response and the properties that make it particularly suitable as a quantitative microscopic imaging technique. CARS microscopy is a four-wave mixing process where a pump field at frequency ω_{pu}, a Stokes field at frequency ω_S, and a probe field at frequency ω_{pr} are focused onto a sample with a high-numerical-aperture (NA) microscope objective. Typically, two laser sources are used, one for the Stokes field and one for both the pump and probe fields, such that $\omega_{pu} = \omega_{pr}$. The temporally and spatially overlapped incident fields interact with the third-order nonlinear susceptibility of the sample, $\chi^{(3)}$. The CARS signal is emitted at the anti-Stokes frequency, $\omega_{AS} = 2\omega_{pu} - \omega_S$, and is collected either in the forward direction or in the epi-direction. $\chi^{(3)}$ describes the material properties of the sample and generally consists of two terms, given by

$$\chi^{(3)} = \chi_R^{(3)} + \chi_{NR}^{(3)} \tag{1}$$

The resonant term, $\chi_R^{(3)}$, reports on vibrational resonances and contains the quantitative and chemically specific information about the sample in the microscope focus, as discussed below.
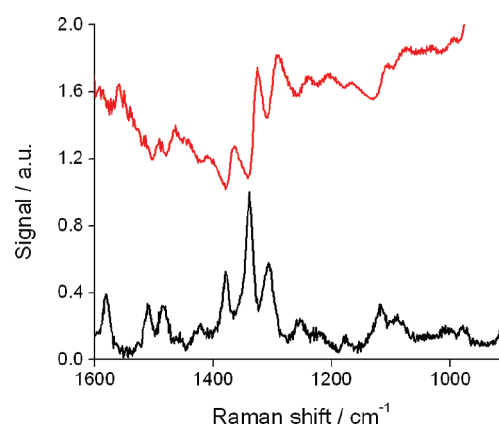

Figure 2. Comparison of (black) spontaneous Raman and (red) multiplex CARS spectra of an equimolar mixture of AMP/ADP/ATP in water at a total concentration of 500 mM. Reproduced from ref 25.

The energy level diagram for the vibrationally resonant response is shown in Figure 1a for a single-frequency CARS experiment. The magnitude of $\chi_R^{(3)}$ is enhanced when the frequency difference between the pump and Stokes beams, $\omega_{pu} - \omega_S$, is resonant with a vibrational transition at frequency Ω of a specific chemical moiety within the sample. In multiplex CARS, a broad range of vibrational transitions are addressed simultaneously by employing a broad-band Stokes beam. The energy level diagram for the resonant response in multiplex CARS is shown in Figure 1b.

The nonresonant response, $\chi_{NR}^{(3)}$, depends solely upon the electronic properties of the material, as shown in Figure 1c. Far from electronic resonances, $\chi_{NR}^{(3)}$ is strictly real and frequency-invariant. However, the magnitude of $\chi_{NR}^{(3)}$ is not spatially invariant throughout a heterogeneous sample; different compositions have different electronic polarizabilities. The detected CARS signal, I_{AS}, depends on both the resonant and nonresonant terms, according to

$$I_{AS} \propto |\chi^{(3)}|^2 = |\chi_R^{(3)} + \chi_{NR}^{(3)}|^2$$

$$= |\chi_R^{(3)}|^2 + 2\chi_{NR}^{(3)} \, \text{Re}[\chi_R^{(3)}] + |\chi_{NR}^{(3)}|^2 \tag{2}$$

CARS is a coherent process; therefore, the resonant and nonresonant responses of the sample interfere via eq 2, and thus, the nonresonant term cannot be retrieved by a simple background correction. It is this interference of the resonant and nonresonant terms that prevents the quantitative data contained within $\chi_R^{(3)}$ from being directly accessible; the presence of the nonresonant contribution, $\chi_{NR}^{(3)}$, to the overall susceptibility means that there is no simple, linear correlation between I_{AS} and concentration. This complexity is illustrated in Figure 2, which shows spontaneous Raman and multiplex CARS spectra of the same sample, an equimolar mixture of AMP/ADP/ATP in aqueous solution at a total concentration of 500 mM.[25] The interference between the nonresonant and resonant terms results in dispersive, Fano-type line shapes in the CARS spectrum in comparison to the Lorentzian-type line shapes in the spontaneous Raman spectrum. Despite the additional complexity of its spectral response, CARS is often preferred to spontaneous Raman thanks to its higher spatial resolution, intrinsic sectioning capability, and its far greater signal; the CARS and Raman spectra in Figure 2 were acquired in 800 ms and 3 min, respectively.

In order to extract the quantitative information from the anti-Stokes CARS intensity I_{AS}, we note that $\chi_R^{(3)}$ probes the
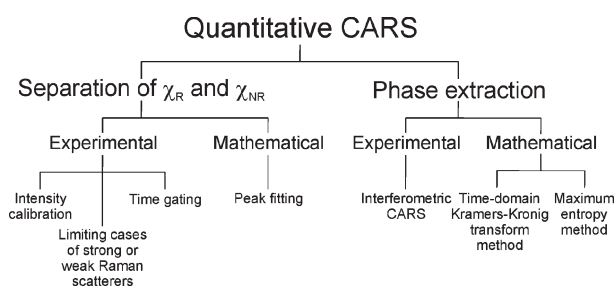
Figure 3. Classification of approaches to quantitative CARS.

Figure 4. Relative CARS intensity at 2913 cm^{-1} for increasing volume fractions of DMSO in water. Reproduced from ref 28.

vibrational response of the material. For one specific vibrational resonance, $\chi_R^{(3)}$ is given by[26]

$$\chi_R^{(3)} = \frac{NA}{\Omega - (\omega_{pu} - \omega_S) - i\Gamma} \tag{3}$$

where A, Ω, and Γ are the amplitude, frequency, and line width of the vibrational mode and N is the number of scatterers per unit volume. For comparison, the spontaneous Raman intensity, I_{Raman}, can be written in the form

$$I_{Raman} \propto \frac{NA\Gamma}{(\Omega - \omega_0)^2 + \Gamma^2} \tag{4}$$

I_{Raman} can be compared directly to the imaginary part of $\chi_R^{(3)}$, given by

$$Im[\chi_R^{(3)}] = \frac{NA\Gamma}{(\Omega - (\omega_{pu} - \omega_S))^2 + \Gamma^2} \tag{5}$$

Crucially, $Im[\chi_R^{(3)}]$ is chemically specific and depends linearly upon concentration.[27] Thus, if we are able to extract $Im[\chi_R^{(3)}]$ from I_{AS}, we can eliminate the complicating influence of the non-resonant term, allowing CARS to be used as a quantitative micro-scopic imaging technique. In fact, additional benefits are obtained by measuring the $Im[\chi_R^{(3)}]$ response. As the $Im[\chi_R^{(3)}]$ spectrum is directly comparable to the spontaneous Raman response of the material, reference can be made to correlation charts of known Raman bands. Second, it is simpler to identify overlapping Lorentzian peaks in an $Im[\chi_R^{(3)}]$ spectrum than the overlapping Fano-type resonances occurring in an I_{AS} spectrum. Finally, as discussed further below, linear analysis techniques can be used to aid spectral deconvolution for complex samples.

Hence, to make CARS quantitative, one has to extract the imag-inary part of the resonant response, $Im[\chi_R^{(3)}]$, from the CARS signal. Because the nonresonant response, $\chi_{NR}^{(3)}$, is instantaneous and therefore purely real, to retrieve $Im[\chi_R^{(3)}]$, it is sufficient if we know the phase of the CARS field, θ, according to

$$Im[\chi_R^{(3)}] = |\chi^{(3)}|\sin\theta \propto \sqrt{I_{AS}}\sin\theta \tag{6}$$

Researchers have developed a number of different approaches to glean quantitative results from CARS data and to deal with the influence of the nonresonant response. For the purposes of this paper, we will classify these approaches into two groups, as shown in the scheme of Figure 3. The first group is comprised of tech-niques that attempt to separate the resonant and nonresonant contributions to the CARS intensity. The second group involves methods that measure or extract the phase in order to retrieve the quantitative $Im[\chi_R^{(3)}]$ response via eq 6. Each group is subdivided into experimental and mathematical approaches.
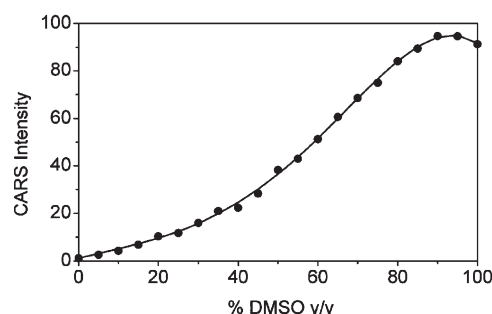
SEPARATION OF THE RESONANT AND NONRESO-NANT RESPONSES

In certain cases, it is possible to extract quantitative informa-tion from the raw CARS signal itself. These approaches aim to access quantitative data quickly for "in-line" analysis. However, they often include significant approximations and assumptions and should be used with care.

Experimental Approaches. *Intensity Calibration.* The sim-plest approach to obtain quantitative data from CARS intensities is to generate a calibration curve that maps from the intensity to analyte concentration. This approach has been used by Zimmerley et al. to follow the penetration of the optical clearing agent dimethyl sulfoxide (DMSO) into skin[28] and to determine the water con-centration in hair.[29] Bergner et al. also used a calibration curve to determine the concentration of deuterated toluene in hydrogenated toluene solutions flowing through a microfluidic device.[30] Although direct and straightforward, the intensity calibration technique is only applicable to the simplest samples. The CARS intensity can vary for a number of reasons besides a change in analyte concentra-tion. Most notably, a change in the local environment surround-ing a species often causes a shift in the resonant frequency of a vibrational mode, Ω, even if the concentration of that species has remained the same. With single-frequency CARS, this peak shift will manifest as a change in intensity and could be misinterpreted as a change in concentration. This potential pitfall was circum-vented by Zimmerley et al. by measuring the calibration curve of DMSO at different concentrations in water, where the peak position of the symmetric methyl vibration is blue-shifted upon dilution.[28] The functional form of their calibration curve shown in Figure 4 is instructive; at low concentrations, the dependence was approxi-mately quadratic, but the curve actually passed through a max-imum CARS intensity at 92 vol %. Evidently, assumption of a specific functional dependence in the absence of a calibration curve is generally best avoided in the quantitative interpretation of CARS data.

Limiting Cases of Strong or Weak Raman Scatterers. Con-centrated samples with a large Raman scattering cross section may approach the limiting case where $\chi_R^{(3)} \gg \chi_{NR}^{(3)}$. Then, eq 2 reduces to $I_{AS} \propto |\chi^{(3)}|^2 \approx |\chi_R^{(3)}|^2$, and the CARS signal depends quadratically on analyte concentration. Heinrich et al. plotted the ratio of the CARS intensities of the vinyl CH stretch and the symmetric CH_2 stretch as a function of unsaturation for a series of vegetable oils and found a quadratic dependence.[31] In the opposite limit of weak or dilute Raman scatterers, $\chi_R^{(3)} \ll \chi_{NR}^{(3)}$. Equation 2 becomes $I_{AS} \propto |\chi^{(3)}|^2 \approx 2\chi_{NR}^{(3)} Re[\chi_R^{(3)}] + |\chi_{NR}^{(3)}|^2$, and the CARS response is linear in concentration with an offset from the strong nonresonant contribution.
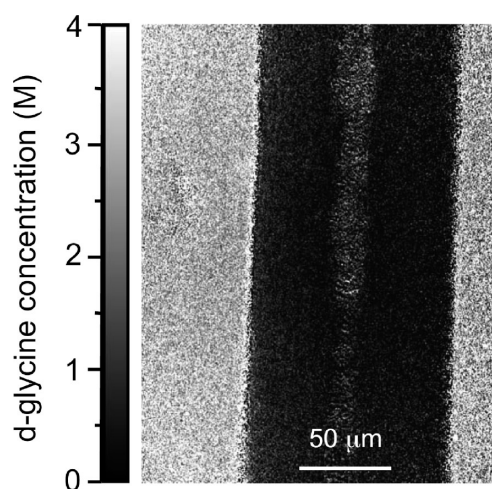
Figure 5. D-Glycine concentration map of a hair immersed in a saturated solution of D-glycine. Reproduced from ref 29.

For a weak Raman scatterer, small changes in the resonant CARS response with concentration can be hard to detect. The sensitivity to variation in concentration can be increased by detecting the CARS response at two different detuning frequencies, $\omega_{pu} - \omega_S$, of the pump and Stokes beams. For an isolated vibrational resonance, the CARS spectrum has both a maximum and minimum due to the interference between $\chi_R^{(3)}$ and $\chi_{NR}^{(3)}$. Taking the ratio[29] or difference[32] between the signals at the maximum and minimum gives a response that is linear in concentration at low concentrations but is not superimposed on a strong background. Zimmerley et al. adopted the ratiometric approach to map quantitatively (Figure 5) the uptake of deuterated glycine into human hair; the ratio was linear in deuterated glycine concentrations up to at least 3.5 M.[29] Li et al. used the differential approach to determine the concentration of deuterated or hydrogenated lipid in a mixed isotope lipid bilayer and found a linear relation across the entire compositional range.[32]

Frequency modulation CARS (FM-CARS) is an extension to the concept of detection at two frequencies. In contrast to the approach presented above, where sequential images are recorded at different detuning frequencies, in FM-CARS, the detuning frequency is modulated rapidly (>500 kHz) between the maximum and minimum to create an amplitude modulation in the CARS intensity. This approach allows for highly sensitive detection by a lock-in amplifier.[33] Chen et al. demonstrated the capabilities of FM-CARS for quantitative analysis to determine the unsaturation composition in mixtures of fatty acids.[34]

Although these approaches are reasonable as quantitative tools in the limit that the resonant term is either very strong or very weak relative to the nonresonant response, some drawbacks may be noted. First, great care must be taken to determine experimentally the extent of these regimes as extrapolation into the intermediate regime will introduce significant error. Furthermore, the dual-frequency approaches (ratiometric, differential, and FM-CARS) make the assumption that the addressed resonance is an isolated peak, which is not always the case. Lastly, in the case of very weak scatterers, the linear relationship with concentration only holds if the magnitude of the nonresonant term is constant throughout the sample, a situation which does not hold in any but the most simple samples.

Time Gating. The spectrally broad nonresonant response and the spectrally narrow resonant response can be separated in the
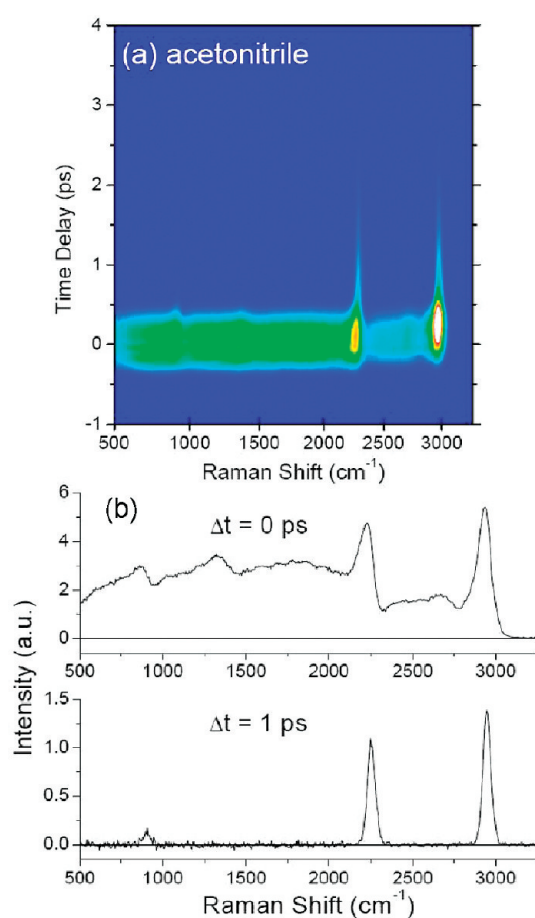

Figure 6. (a) Time-resolved CARS spectra of acetonitrile. (b) CARS spectra at delay times of 0 and 1 ps. Reproduced from ref 35.

time domain. The purely real nonresonant response will follow directly the driving field; it vanishes as the driving field vanishes. The resonant response, in contrast, exhibits a finite dephasing time; the vibrational coherence set up by the pump and Stokes pulses will extend over several picoseconds depending upon the line width of the vibrational mode. The difference in the dephasing times can be used to separate the information-rich resonant response from the nonresonant response, as exemplified in Figure 6. At a time delay of 0 ps, the CARS spectrum of acetonitrile exhibited distinctive dispersive resonances, but here, the introduction of a delay of 1 ps eliminated the effect of the nonresonant contribution, and the signal depends solely on the resonant response.

The time-grating approach to CARS microscopy was first employed by Volkmer et al.[36] Their optical scheme employed three optical fields. The pump and Stokes beams induced nonlinear polarization in the sample, which was allowed to decay partially before being upconverted into a CARS signal by the probe beam. The workers were thus able to image polystyrene beads in the absence of the nonresonant term. Other groups have also employed the time gating approach to remove the nonresonant contribution, either based on a two-pulse setup[35] or a single-pulse setup with pulse shaping,[37] but none have used this scheme explicitly for a quantitative study. It should be noted that by excluding the nonresonant signal, one is also negating the amplification effect of the nonresonant contribution (from the cross-term in eq 2), and signals are accordingly weaker. Furthermore, in
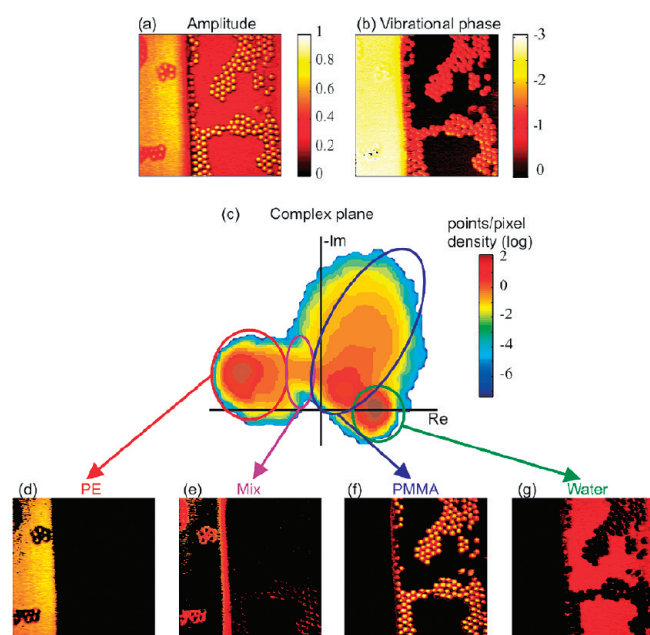
Figure 7. Measurement of the amplitude and phase in a sample allows identification of the individual components. (Top) Amplitude (a) and vibrational phase (b) of a sample containing a sheet of PE, 4 μm PMMA beads, and water, imaged at 2940 cm^{-1}. (Middle) Density graph of the projected amplitude and vibrational phase points in the complex plane (c). (Bottom) Multicomponent analysis, where the different components (d–g) are separated by their location in the complex plane. The "mix" plot shows regions of the image where all three components are represented in the same focal volume. Each image is 100 μm × 100 μm. Reproduced from ref 49.

order to extract quantitative information from time-gated spectra, it is necessary to correct for the different line widths of the different vibrational modes. The amplitudes of broader peaks will decay more rapidly in time, as evinced in Figure 6b, where the broad resonance centered at ∼1400 cm^{-1} at $\Delta t = 0$ is no longer visible at $\Delta t = 1$ ps. One would therefore have to measure the intensity of the resonant signal as a function of time for finite delay and extrapolate to 0 to obtain quantitative data and allow for a quantitative comparison between resonances of different line widths. These issues may explain why this technique has not been used explicitly as a quantitative probe.

Mathematical Approaches. *Peak Fitting.* This approach makes the assumption that $\chi_{NR}^{(3)}$ is purely real, positive, and frequency-invariant. The number of vibrational resonances within a spectrum is either estimated or measured by spontaneous Raman spectroscopy, and the CARS response is modeled according to eqs 2 and 3, with $\chi_{NR}^{(3)}$, A, Ω, and Γ as fitting parameters, with the latter three parameters appearing for each resonance.[38,39] The concentration of a species is then proportional to A in the event that the vibrational resonance is unique for that species. If the spontaneous Raman spectrum is available and relatively simple, this approach works well, and it has been successfully used to determine the chain order in phospholipid mono- and bilayers,[40] to resolve the nucleotide concentrations in mixtures[41] and to image quantitatively the composition of polymer blends.[42] Although this approach is straightforward, estimating the number of vibrational resonances in any but the simplest spectra is nontrivial without the aid of the corresponding spontaneous Raman spectrum. Furthermore, in complex samples, the tail of a strong resonant

peak can be mistakenly identified as a nonresonant contribution.[43] Consequently, this approach has been largely superseded by the phase retrieval methods described below, which do not require a priori information about the vibrational spectrum.

PHASE EXTRACTION

As discussed above, Im$[\chi_R^{(3)}]$ is linearly proportional to the concentration of a chemical species. According to eq 6, Im$[\chi_R^{(3)}]$ can be obtained from the CARS signal intensity if the vibrational phase of the CARS signal is known. Physically, the vibrational phase is the difference between the driving field (the superposition of the pump and Stokes fields) and the motion of the dipoles in the sample. The nonresonant response has zero phase as it is real, positive, and instantaneous, but the resonant response has a nonzero vibrational phase whose magnitude will vary depending on the detuning frequency, $\Omega - (\omega_{pu} - \omega_S)$, and the concentration of the sample. Very dilute samples ($\chi_R^{(3)} \ll \chi_{NR}^{(3)}$) will have a vibrational phase close to 0, whereas for highly concentrated samples, the phase shift can increase up to π radians. The vibrational phase can be measured experimentally or extracted mathematically from the CARS signal intensity.

Experimental Approaches. *Interferometric CARS.* Conventional power detectors such as photomultipliers (PMTs) and charge-coupled devices (CCDs) measure the intensity of incident light and hence are unable to measure the phase of the CARS signal directly. The vibrational phase can be measured on a PMT or CCD by mixing interferometrically the CARS field, E_{AS}, with a reference pulse with a well-defined phase relationship to the CARS field (the so-called local oscillator field, E_{LO}).

The total intensity on the detector, I_{det}, is given by[44]

$$I_{det} = |E_{LO} + E_{AS}|^2 = |E_{LO}|^2 + |E_{AS}|^2 + 2|E_{LO}E_{AS}| \cos \phi \tag{7}$$

and ϕ is the phase difference between the CARS field and the local oscillator field. Once the vibrational phase is known, the quantitative Im$[\chi_R^{(3)}]$ response can be determined.

Potma et al. have used interferometric CARS to image the Im$[\chi_R^{(3)}]$ response of live cells.[45] They also demonstrated the linearity of the heterodyned interferometric signal as a function of concentration for solutions of dodecane in deuterated dodecane. In their design, the local oscillator was derived from the nonresonant response in deuterated DMSO. Jurna et al. developed an alternative design in which the local oscillator originated from the same optical parametric oscillator (OPO) as the Stokes beam such that all pulses in the system were inherently phase-locked in a phase-preserving chain.[46] Von Vacano et al. used pulse shaping to implement a single-beam approach to interferometric CARS and demonstrated the linearity of the interferometric signal as a function of concentration for solutions of bromoform in ethanol, although the sampling rate was limited to 700 Hz by the use of a lock-in detector.[47] Chowdary et al. demonstrated the quantitative analytical capabilities of interferometric CARS by comparing the level of unsaturation in different vegetable oils. The level of unsaturation was determined empirically by an independent iodine assay and spectroscopically by interferometric CARS and spontaneous Raman spectroscopy; both interferometric CARS and Raman displayed a linear dependence.[48] They also mapped quantitatively the lipid and protein composition within a section of pig tissue.
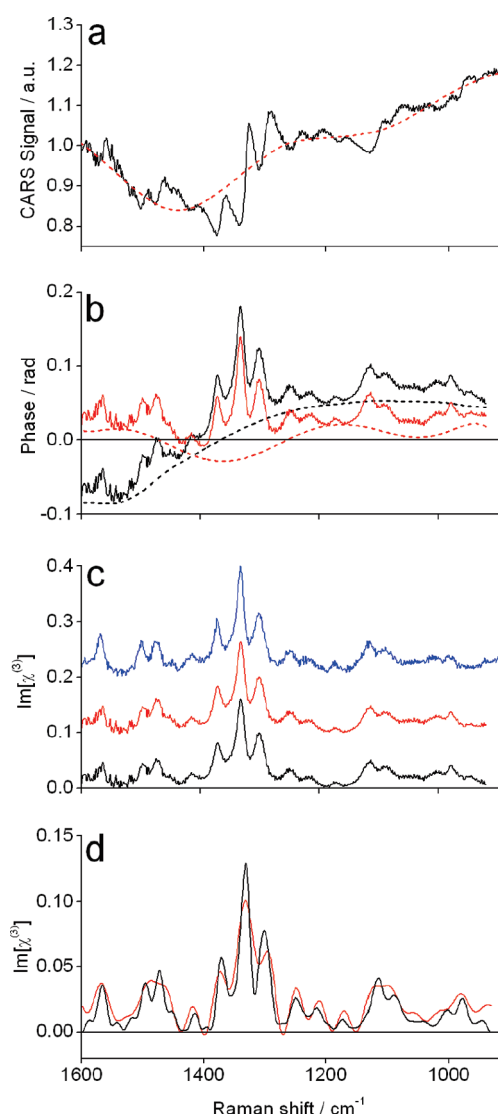
Figure 8. Retrieval of phase and $Im[\chi_R^{(3)}]$ from CARS spectra by the time-domain Kramers—Kronig (TD-KK) transform and the maximum entropy method (MEM). (a) Multiplex CARS spectrum of an equimolar mixture of AMP/ADP/ATP in water at a total concentration of 500 mM (solid black line, from Figure 2) and estimation of the nonresonant background for TD-KK (red, dotted line). (b) Phase retrieved with $N = 256$ autocorrelations by the MEM (solid black line), TD-KK (solid red line), error phase for the MEM phase (dotted black line), and error phase for the TD-KK phase (dotted red line). (c) $Im[\chi_R^{(3)}]$ spectra retrieved with $N = 256$ autocorrelations by MEM (solid black line), TD-KK (solid red line), and the Raman spectrum of the same solution (solid blue line, from Figure 2). The spectra are offset for clarity. (d) $Im[\chi_R^{(3)}]$ spectra retrieved with $N = 35$ autocorrelations by MEM (solid black line) and TD-KK (solid red line).

CARS microscopy is often used to study complex samples, where the spectrum consists of many overlapping vibrational resonances. If there are two or more species in the sample that have overlapping resonances, it is not generally possible with single-frequency CARS to determine the relative amounts of these species in the sample. However, Jurna et al. have demonstrated that by measuring both the vibrational phase and the amplitude of the CARS signal at a single frequency, it is possible to discriminate between species with overlapping resonances without employing

a multiplex approach. They were able to separate the responses of PE, PMMA, and water in the complex plane in order to distinguish these species, as shown in Figure 7.[49]

Interferometric CARS offers an attractive route to quantitative CARS measurements; by measuring the phase directly, this technique does not rely on the assumptions implicit in the mathematical approaches to phase retrieval (vide infra). Furthermore, the local oscillator intensity can be increased to amplify weak signals (eq 7). However, the apparatus required is necessarily more complex and requires interferometric stability, which may preclude the use of these techniques outside of the dedicated laser lab.

Mathematical Approaches. Although PMTs and CCDs in a noninterferometric CARS experiment only measure the intensity of the CARS signal (the power spectrum), it is still possible to retrieve an approximation to the vibrational phase mathematically from the CARS signal. This is the classical phase retrieval problem, how to recover the phase of a complex function from its modulus. This problem is encountered across many different scientific fields, including crystallography,[50] astronomy, and linear and nonlinear spectroscopy.[51] Although in the most general case there are an infinite number of solutions to the phase retrieval problem, in any practical situation, there are constraints on the form of the solution.[50] These constraints reduce drastically the number of allowed solutions and, in the case of CARS spectra, typically result in a very good approximation to the real vibrational phase. The retrieved phase can then be used to calculate the $Im[\chi_R^{(3)}]$ spectrum via eq 6. Two well-established approaches to mathematical phase retrieval of CARS spectra are the time-domain Kramers—Kronig (TD-KK) transform and the maximum entropy method (MEM). First, we describe the underlying principles and applications of these approaches, before discussing their respective advantages and limitations.

Time-Domain Kramers—Kronig (TD-KK) Transform Method.
The vibrational phase spectrum can be retrieved from an intensity spectrum by the Kramers—Kronig transform, given by[52]

$$\theta(\omega) = -\frac{P}{\pi} \int_{-\infty}^{\infty} \frac{\ln |I_{AS}(\omega')|}{\omega' - \omega} \, d\omega' \qquad (8)$$

where P is the Cauchy principal value. However, eq 8 requires that the intensity spectrum be known across an infinite frequency range, a situation that is never realized in practice. Although the intensity spectrum can be extrapolated beyond the measured frequency range, eq 8 is very sensitive to the nature of this extrapolation. Therefore, the Kramers—Kronig transform in the frequency domain may not be the most suitable approach to retrieve the vibrational phase spectrum from a CARS spectrum. However, if there are no spectral features at the edges of the frequency window, the phase can be retrieved with limited data via a Fourier transform into the time domain, given by[52]

$$\theta(\omega) = \begin{cases} 2Im\left\{ \mathscr{T}(\mathscr{T}^{-1}[\ln |I_{AS}(\omega)|]) - \dfrac{\ln |I_{AS}(\omega)|}{2} \right\} & t \geq 0 \\[2ex] 2Im\left\{ \mathscr{T}(\mathscr{T}^{-1}[\ln |I_{NR}(\omega)|]) - \dfrac{\ln |I_{NR}(\omega)|}{2} \right\} & t < 0 \end{cases}$$

$$(9)$$

where $\mathscr{T}$ and $\mathscr{T}^{-1}$ indicate the Fourier and inverse Fourier transform and I_{NR} is the nonresonant response. Sung et al. have demonstrated that the $Im[\chi_R^{(3)}]$ spectra retrieved in this manner are linear in concentration for a series of Na_2SO_4 solutions.[53] Parekh et al. have employed the TD-KK approach to extract

G

dx.doi.org/10.1021/jp200606e |*J. Phys. Chem. B* XXXX, XXX, 000–000

$Im[\chi_R^{(3)}]$ spectra from mouse fibroblast cells. They were able to differentiate and image the nuclear and the cytoplasmic regions of the cells based on their vibrational spectra alone.[54]

Maximum Entropy Method (MEM). The MEM also retrieves the phase spectrum from the intensity spectrum mathematically, but here, the phase retrieval is based on the maximum entropy principle. We will briefly outline the philosophy behind this principle before describing its application to analyze CARS spectra.

As discussed above, a CARS spectrum is generally only known over a limited frequency range. In the time domain, this statement is equivalent to the fact that only a limited number of auto-correlations are known. The MEM provides a practical approach to fit a measured CARS spectrum based on this limited number of autocorrelations and, at the same time, retrieve the phase. Using this method, one can extract an estimated vibrational phase from the CARS spectrum with no prior assumptions and no fitting parameters. The application of MEM to CARS spectra benefits greatly from the availability of multiplex CARS spectra and has therefore recently attracted renewed attention. We refer the interested reader to the literature for a thorough description of the mathematics of the MEM[25,27,51,55] and focus here on its use.

The ability of the MEM to retrieve the $Im[\chi_R^{(3)}]$ spectrum has proven to be particularly useful in cellular biology studies. The fingerprint region ($\sim 800-1800$ cm^{-1}) is especially rich in information, but peak identification is considerably easier from $Im[\chi_R^{(3)}]$ spectra than from raw CARS spectra. Petrov et al. were able to identify bands from calcium dipicolinate within individual *Bacillus subtilis* endospores.[56]

Comparison of the TD-KK and MEM. The MEM and TD-KK methods are closely linked; both approaches aim to retrieve the vibrational phase and ultimately yield an approximation to the true $Im[\chi_R^{(3)}]$ spectrum. In this section, we shall compare these two approaches to phase retrieval by analyzing the CARS spectrum of the sample from Figure 2. This spectrum and its phase retrieval by each method are shown in Figure 8.

CARS spectra are typically complicated by the presence of a nonresonant background that is not spectrally flat. This non-constant background arises from the convolution of the pump and Stokes pulses[52] and is exemplified in Figure 8a. In the TD-KK approach, this nonconstant background must be estimated in the CARS spectrum (red dotted line, Figure 8a). There are techniques that allow an estimation of this nonconstant background based on iteration[57] or the wavelet transform, but nonetheless, estimating the nonconstant background in the CARS spectrum is nontrivial. In contrast, the MEM does not require such an estimate to the nonconstant background in the CARS spectrum.

The phase spectra retrieved by each approach are shown in Figure 8b. In the MEM, the effect of the nonconstant background in Figure 8a manifests as a slowly varying background to the phase in Figure 8b. For weak or dilute Raman scatterers, $\chi_R^{(3)} < \chi_{NR}^{(3)}$, the true phase must be zero away from vibrational resonances, according to[25]

$$\theta = \tan^{-1}\left(\frac{Im[\chi_R^{(3)}]}{\chi_{NR}^{(3)} + Re[\chi_R^{(3)}]}\right) \approx 0 \qquad (10)$$

In this limit, the slowly varying background (the error phase) is a straightforward polynomial background correction to the retrieved phase, as demonstrated in Figure 8b (black dotted line). The phase spectrum retrieved by the TD-KK approach also requires an error phase correction (red dotted line), arising from inaccuracies in the estimation of the nonresonant background.

Background correction is of course well-known in Raman and IR spectroscopy, and a number of well-defined approaches exist.

The $Im[\chi_R^{(3)}]$ spectra retrieved by each approach are shown in Figure 8c and compared to the Raman spectrum of the same sample. It is evident that both approaches retrieve the correct line shapes and line widths equally well; the only differences between the two $Im[\chi_R^{(3)}]$ spectra arise from subtle differences in the error phase fitting in Figure 8b.

From a computational point-of-view, the TD-KK approach involves a series of Fourier transforms that require $O(N \log N)$ operations, where N is the number of autocorrelations. The MEM employs both Fourier transforms and the solution of a Toeplitz system of coupled linear equations and hence requires $O(N^2)$ operations. The $Im[\chi_R^{(3)}]$ spectra in Figure 8c were retrieved by using $N = 256$ autocorrelations, such that the TD-KK approach is ~ 50 times faster than the MEM in this case. However, in Figure 8d, the $Im[\chi_R^{(3)}]$ spectra were retrieved with $N = 35$. All of the spectral features are satisfactorily recovered by the MEM (indeed, the use of fewer autocorrelations also leads to a reduction in high-frequency noise),[27] whereas peak broadening has occurred for the TD-KK with 35 autocorrelations. Hence, in reality, both approaches can retrieve the phase equally rapidly.

In conclusion, there is little difference in the effectiveness of each phase retrieval method; both methods allow for quantitative analysis of CARS spectra. The MEM approach, however, does have the slight advantage that no estimate of the nonconstant background is required, and high-frequency noise can be eliminated by use of fewer autocorrelations.

The congested spectra from a hyperspectral approach (derived from either spontaneous or coherent Raman scattering) are likely to require further analysis to access useful information. Here, a further advantage that arises from converting I_{AS} spectra to $Im[\chi_R^{(3)}]$ spectra is that the legion of spectral analysis techniques that have been developed to help analyze congested linear spectra (such as principal component analysis) can now be brought to bear upon CARS spectra. A detailed review of this large field is beyond the scope of this article, and we refer the reader elsewhere for a comprehensive review,[58] but we will briefly describe some of the most useful chemometric approaches.

The simplest approach to deconvolute overlapping spectral features from multicomponent mixtures occurs when the pure spectra of the individual components are known in advance. In this case, each spectrum in the hyperspectral image is treated as a linear combination of the pure spectra, and the resulting linear coefficients are proportional to the concentration of each component in that spectrum. Constraints to remove unphysical results such as negative concentrations can also be included.[59] More sophisticated approaches typically employ the singular-value decomposition, which decomposes the multivariate data set into abstract components that are ordered to express decreasing variance of the data. Consequently, only the first few abstract components contain real spectral information, and the rest can be discarded, reducing the noise in the data set.[60] Procedures such as target factor analysis,[61] alternating least-squares,[58] or band-target entropy minimization[62] can then be employed to rotate the abstract components back into real spectra and compositions.

For biological samples, the vibrational spectra can be so complex that it is not possible to isolate the response of an individual molecular species throughout a sample. In these instances, cluster analysis is a useful approach to examine hyperspectral images. Cluster analysis attempts to group together regions within an

H

dx.doi.org/10.1021/jp200606e |*J. Phys. Chem. B* XXXX, XXX, 000–000

image that exhibit similar spectral features, such as tissue structures[63] or cellular organelles.

Applications of the MEM. We have used the MEM extensively within our groups to study a range of questions in both life science and materials science. Microfluidic devices are ideal reaction vessels for the production of fine chemicals, allowing unprecedented control over the interaction of reagents. However, in order to fully
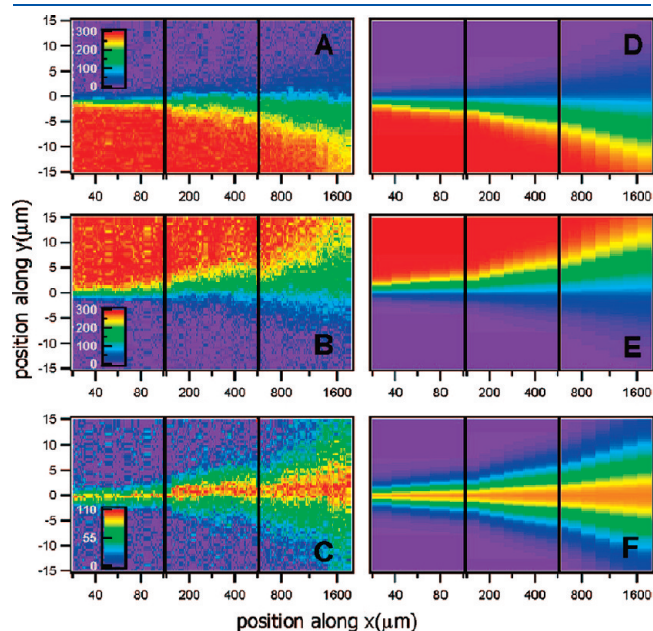

Figure 9. Concentration profiles of (A) pyrrolidine, (B) acetic acid, and (C) their reaction product within a microfluidic device. Panels (D−F) provide the corresponding results of a numerical simulation. Reproduced from ref 16.
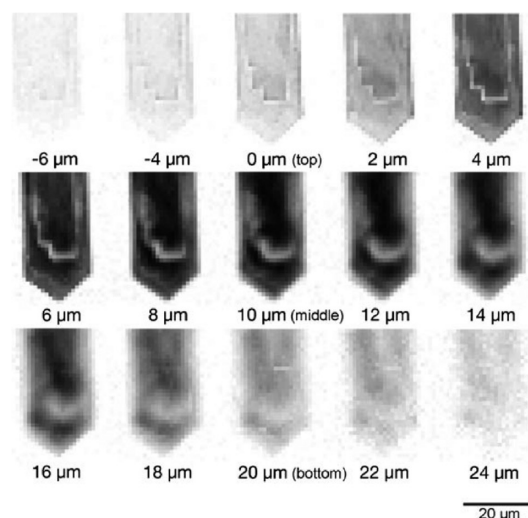

Figure 10. CARS images of the normalized concentration of 2-chlorothiophene in an H-ZSM-5 zeolite crystal. Reproduced from ref 15.
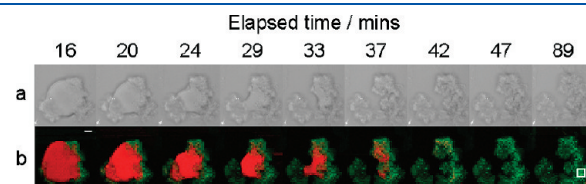

Figure 11. Time-resolved images of the digestion of a glyceryl trioleate droplet by porcine pancreatic lipase. (a) Bright-field microscopy images. (b) False-color images obtained by CARS microspectroscopy of glyceryl trioleate (red) and lipolytic products (green). Scale bar = 5 μm; pixel step size = 1 μm. Reproduced from ref 65.
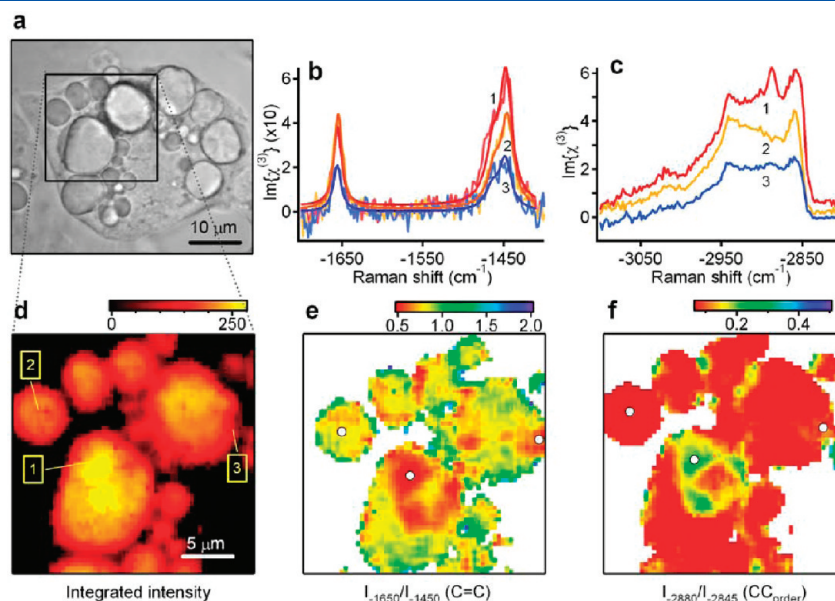

Figure 12. (a) Brightfield image of an adipocyte incubated with a 1:3 mixture (mol:mol) of LA and PA. The marked region was imaged with multiplex CARS microscopy. On the basis of the measured $\text{Im}[\chi_R^{(3)}]$ spectra at every pixel, images are derived with the contrast based on (d) lipid concentration (integrated intensity), (e) C=C concentration derived from the CC stretch region (I-1650/I-1450), and (f) acyl chain order (I-2880/I-2845). In (b) and (c), representative $\text{Im}[\chi_R^{(3)}]$ spectra are shown recorded at the locations indicated in (d) for the CC stretch and CH stretch spectral regions, respectively. The least-squares fit of a sum of three Lorentzians to the data is also shown in (b). The acquisition time was 20 ms for a multiplex CARS spectrum at every pixel position (~1 min/image). Reproduced from ref 66.

I

dx.doi.org/10.1021/jp200606e |*J. Phys. Chem. B* XXXX, XXX, 000–000

exploit the capabilities of microfluidic chips, quantitative on-chip monitoring of fluid flow, mixing, and reaction rates is required. We have shown that it is possible to quantify the local concentrations of miscible fluids within a microfluidic device using CARS microscopy. In the case of nonreacting species, this information reports on the mass transport within the device and can potentially be used to determine unknown diffusion coefficients or fluid flow behavior in shear-sensitive media.[64] In the case of reacting species, the local concentration images that are determined by quantitative CARS microscopy can be used to investigate fast reaction kinetics. As an example, we studied the rapid proton transfer between acetic acid and pyridine. As shown in Figure 9, we mapped the concentration of each species throughout the chip, and by fitting the concentration data to a reaction-diffusion model, we were able to determine a lower limit for the rate constant of this reaction.[16] The ability to determine local concentration profiles within a microfluidic device with quantitative CARS microscopy also lends itself to studies of the physical chemistry of fast reactions that are catalyzed by homogeneous catalysts.

We have also used quantitative CARS to study reactions in heterogeneous catalysts, namely, in zeolite crystals. The inherent confocality, (sub)micrometer spatial resolution, and high sensitivity render the CARS approach ideal for the study of the interplay between catalyst architecture and molecular reaction and gain hitherto inaccessible information about fundamental processes in catalysis. As an example, we have studied precursor states of thiophene conversion over individual H-ZSM-5 zeolite crystals. Chemical maps (Figure 10) of the loaded catalysts revealed a nonhomogeneous, diffusion-limited distribution of 2-chlorothiophene throughout the crystal, where the analyte accumulates in the center of the crystal and along defect sites The diffusion of molecules across crystal phase boundaries appeared to be strongly hindered. CARS has the potential to become a valuable tool also for the characterization of catalysts during reaction cycles.[15]

Enzyme-catalyzed hydrolysis is a key step in the digestion and uptake of lipids by the human gastrointestinal tract. We used quantitative CARS microscopy to follow the digestion of an emulsion of the unsaturated lipid glyceryl trioleate in a model system, and we were able to distinguish readily between the digested and undigested species, as shown in Figure 11. Furthermore, we quantified the local concentrations and distributions of progesterone and vitamin D_3 within emulsion droplets of the saturated lipid glyceryl trioctanoate during digestion.[65] Such data is essential to optimize formulations for the delivery of bioactive ingredients and lipid-soluble drugs.

The fatty acids produced during the digestion process are absorbed by adipocytes and converted back into triacylglycerides. These triacylglycerides are stored within the cell in organelles
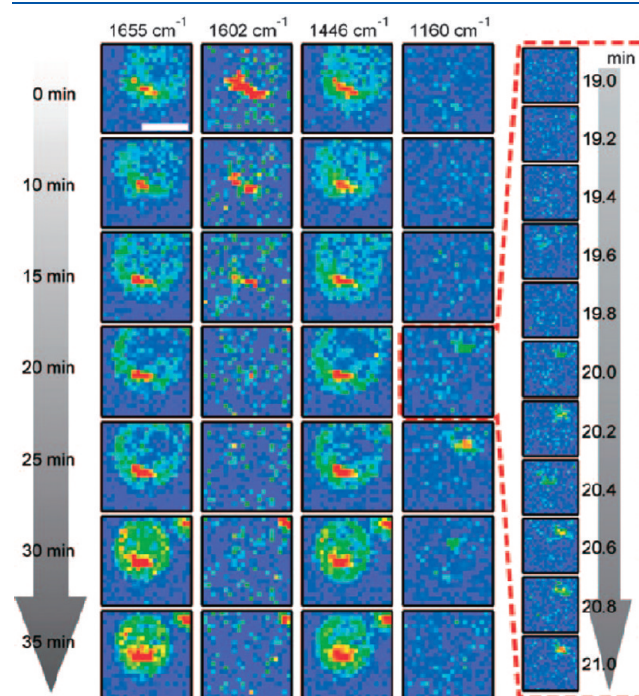

Figure 13. Time-resolved CARS images of the Raman bands at 1655, 1602, 1446, and 1160 cm^{-1}, respectively. The scale bar inside of the image is 5 μm. The color scale for each band is the same for all of the times measured. The red frame on the right contains CARS images at 1160 cm^{-1} from 19 to 21 min. Each image is measured every 12 s. Each of the seven rows of images is constructed from Raman intensities retrieved from one CARS spectrum. Reproduced from ref 60.

Table 1. Table Comparing the Strengths and Weaknesses of the Approaches to Quantitative CARS Microscopy Described in the Text

technique	strengths	weaknesses	single-frequency or multiplex
intensity calibration	rapid, simple, low calculation cost	subject to artifacts when images acquired in different environment to calibration data	both
limiting case of strong or weak raman scatterers	rapid, simple, low calculation cost	subject to artifacts in intermediate regime	both
time gating	linear response	no amplification from nonresonant term dependence on line widths of different vibrational modes	both
peak fitting	rapid, low calculation cost	requires prior knowledge of peaks	multiplex
interferometric CARS	directly measure Im$[\chi_R^{(3)}]$	complex experimental setup	both
time-domain Kramers–Kronig transform	no a priori knowledge of peak shapes necessary	estimation of nonresonant background necessary error phase correction necessary	multiplex
MEM	no a priori knowledge of peak shapes necessary	error phase correction necessary	multiplex

known as lipid droplets. We used CARS microscopy to image such lipid bodies in mouse adipocyte cells incubated with different mixtures of saturated (palmitic acid, PA) and unsaturated (linolenic acid, LA) fatty acids.[66] The high level of information contained within the vibrational spectra allowed us to determine quantitatively not only the composition but also the distributions of the fluidity and degree of unsaturation within the lipid droplets, as shown in Figure 12.

The interpretation of vibrational spectra acquired from within cells is challenging as the signals are often weak and the spatial variations in composition are subtle. Okuno et al. acquired CARS spectra of a budding yeast cell spanning the entire fingerprint range $(800-1800 \text{ cm}^{-1})$ and employed the MEM to retrieve the $\text{Im}[\chi_R^{(3)}]$ spectra. $\text{Im}[\chi_R^{(3)}]$ spectra are linear and, hence, were amenable to noise reduction by the singular value decomposition (SVD). The combination of a broad-band laser source, the MEM, and noise reduction by the SVD allowed the identification of features in the spectra that were used to give simultaneous time-lapse images of the behavior of mitochondrial phospholipids, proteins, and a vacuole dancing body within the budding yeast cell, as shown in Figure 13.[60]

■ SUMMARY

CARS microscopy offers an attractive route to quantitative microscopy. Different species within a sample can be distinguished in a label-free manner based on their vibrational signatures, and the local concentration of each species can be obtained down to mM concentrations, or to μM concentrations with electronic resonant enhancement.[67] Such capabilities are likely to become increasingly important as researchers aim to progress to quantitative descriptions of processes occurring at submicrometer length scales.

Many approaches have been developed to access the quantitative information within the CARS signal, although none of the approaches described above can lay claim to be the best solution in all cases. Each approach has its own strengths and weaknesses, which we list in Table 1. Using these approaches, it is nearly always possible to obtain some quantitative data about a sample with CARS microscopy. Generally, the two most difficult types of samples to study are (i) those in which the concentration of the species of interest is low and (ii) the complex samples that give rise to congested vibrational spectra. The further development of tools that are able to address these situations is likely to prove indispensable.

■ BIOGRAPHIES

James P. R. Day received a Master's degree in Chemistry from the University of Oxford in 2004, where his final year project involved the use of infrared spectroscopy to study the adsorption kinetics of surfactants. After completing his Ph.D. in 2008 at Durham University on the development of spectroscopic techniques to study adsorption to the oil—water interface, James moved to Amsterdam to begin a postdoctoral position at the FOM Institute AMOLF. His work currently concerns the application of CARS microscopy to study the bioavailability of nutriceuticals during digestion, as well as proton and water transport in fuel cell membranes.

Katrin F. Domke completed her diploma thesis in electrochemistry in 2004 at the University of Bonn and moved to the Fritz Haber Institute in Berlin where she carried out her Ph.D. studies on tip-enhanced Raman spectroscopy. Her thesis was awarded the Wilhelm-Ostwald Nachwuchspreis 2007. Katrin has been a Feodor Lynen Postdoc in the group of Prof. Bonn at FOM Institute AMOLF in Amsterdam since 2008. Her main research interest lies in elucidating the correlation between architecture and catalytic activity of zeolite crystals with multiplex CARS spectromicroscopy.

Gianluca Rago obtained his M.Sc. degree in condensed matter physics in Parma, performing as well research projects in Leiden and Durham. Since December 2007, Gianluca is a Ph.D. student at the FOM Institute AMOLF, where he is working on the applications of nonlinear optical techniques, primarily single-line and multiplex CARS as well as two-photon fluorescence in biomedicine and chemistry. His research currently concerns the study of the kinetics of catalytic chemical reactions and the interactions of nanostructures with cells.

Hideaki Kano is currently an Associate Professor of the Graduate School of Science, the University of Tokyo. He graduated from the Department of Physics, School of Science at the University of Tokyo in 1996. He received his M.Sc. and D.Sc. from the University of Tokyo in 1998 and 2001, respectively. He was appointed Research Associate at the University of Tokyo in 2001 and was promoted to his present position in 2007. Since 2007, he has been a PRESTO researcher of the Japan Science and Technology Agency (JST). His research interests involve developing spectroscopic methods using novel nonlinear optical processes for imaging biological molecules in living cells and organisms at the molecular level.

Hiro-o Hamaguchi is a Professor at the Department of Chemistry, School of Science at the University of Tokyo. He received his B.Sc. Degree from the University of Tokyo in 1970 and his D.Sc. Degree in physical chemistry from the same university in 1975. He was guided to the research field of vibrational spectroscopy by romantic phrases, "Spectra are letters from the molecule" and "Vibrational spectra are molecular fingerprints". His recent research efforts are directed toward the elucidation of complex molecular systems including solutions and liquids, ionic liquids, and also living cells and human organs, using time- and space-resolved vibrational spectroscopy.

Erik M. Vartiainen received his M.Sc. and Ph.D. degrees in physics from the University of Joensuu in 1988 and 1993, respectively. From 1991 to 1993, he worked at Professor Toshimitsu Asakura's laboratory, at the Hokkaido University, Japan. Since 1993, he has been working at the Laboratory of Physics, Lappeenranta University of Technology (LUT), in various positions, including a 5 year professorship in physics. Currently, he is an adjunct professor in optical physics. During 2006—2008, he was the chairman of the Finnish Optical Society (FOS). He is an author of 2 monographs on optical spectroscopy and 50 original articles. His research interests include optical spectroscopy, optical engineering, and nonlinear optics.

Mischa Bonn received his Ph.D. in 1996 for work resulting from a collaboration between the Technical University of Eindhoven (Rutger van Santen) and AMOLF (Aart Kleyn/Huib Bakker). After postdoctoral work at the Fritz-Haber Institute in Berlin (Martin Wolf and Gerhard Ertl) and Columbia University in New York (Tony Heinz), Mischa worked at the chemistry department at Leiden University (1999-2004), before moving to AMOLF (2004), where he heads the "Biosurface Spectroscopy" group. Mischa received the 2009 Gold Medal from the Royal Dutch Chemical Society and holds a professorship at the Physics faculty of the University of Amsterdam.

K

dx.doi.org/10.1021/jp200606e |J. Phys. Chem. B XXXX, XXX, 000–000

■ ACKNOWLEDGMENT

■ REFERENCES

(1) Peibois, C. *Anal. Bioanal. Chem.* **2010**, *397*, 2051–2065.

(2) Rittweger, E.; Han, K. Y.; Irvine, S. E.; Eggeling, C.; Hell, S. W. *Nat. Photonics* **2009**, *3*, 144–147.

(3) Furtado, A.; Henry, R. *Anal. Biochem.* **2002**, *310*, 84–92.

(4) Fahrni, C. J. *Curr. Opin. Chem. Biol.* **2007**, *11*, 121–127.

(5) MacAleese, L.; Stauber, J.; Heeren, R. M. A. *Proteomics* **2009**, *9*, 819–834.

(6) Heeren, R. M. A.; Kukrer-Kaletas, B.; Taban, I. M.; MacAleese, L.; McDonnell, L. A. *Appl. Surf. Sci.* **2008**, *255*, 1289–1297.

(7) Petibois, C.; Deleris, G.; Piccinini, M.; Cestelli, G. M.; Marcelli, A. *Nat. Photonics* **2009**, *3*, 179.

(8) Zumbusch, A.; Holtom, G. R.; Xie, X. S. *Phys. Rev. Lett.* **1999**, *82*, 4142–4145.

(9) Duncan, M. D.; Reintjes, J.; Manuccia, T. J. *Opt. Lett.* **1982**, *7*, 350–352.

(10) Hellerer, T.; Axang, C.; Brackmann, C.; Hillertz, P.; Pilon, M.; Enejder, A. *Proc. Natl. Acad. Sci. U.S.A.* **2007**, *104*, 14658–14663.

(11) Balu, M.; Liu, G.; Chen, Z.; Tromberg, B. J.; Potma, E. O. *Optics Express* **2010**, *18*, 2380–2388.

(12) Nan, X. L.; Potma, E. O.; Xie, X. S. *Biophys. J.* **2006**, *91*, 728–735.

(13) Evans, C. L.; Xie, X. S. *Annu. Rev. Anal. Chem.* **2008**, *1*, 883–909.

(14) Camp, C. H.; Yegnanarayanan, S.; Eftekhar, A. A.; Sridhar, H.; Adibi, A. *Optics Express* **2009**, *17*, 22879–22889.

(15) Kox, M. H. F.; Domke, K. F.; Day, J. P. R.; Rago, G.; Stavitski, E.; Bonn, M.; Weckhuysen, B. M. *Angew. Chem., Int. Ed.* **2009**, *48*, 8990–8994.

(16) Schafer, D.; Squier, J. A.; van Maarseveen, J.; Bonn, D.; Bonn, M.; Muller, M. *J. Am. Chem. Soc.* **2008**, *130*, 11592–11593.

(17) Evans, C. L.; Xu, X.; Kesari, S.; Xie, X. S.; Wong, S. T. C.; Young, G. S. *Optics Express* **2007**, *15*, 12076–12087.

(18) Evans, C. L.; Potma, E. O.; Puoris'haag, M.; Cote, D.; Lin, C. P.; Xie, X. S. *Proc. Natl. Acad. Sci. U.S.A.* **2005**, *102*, 16807–16812.

(19) Cui, M.; Bachler, B. R.; Ogilvie, J. P. *Opt. Lett.* **2009**, *34*, 773–775.

(20) Freudiger, C. W.; Min, W.; Saar, B. G.; Lu, S.; Holtom, G. R.; He, C.; Tsai, J. C.; Kang, J. X.; Xie, X. S. *Science* **2008**, *322*, 1857–1861.

(21) Nandakumar, P.; Kovalev, A.; Volkmer, A. *New J. Phys.* **2009**, *11*, 033026.

(22) Ploetz, E.; Laimgruber, S.; Berner, S.; Zinth, W.; Gilch, P. *Appl. Phys. B: Laser Opt.* **2007**, *87*, 389–393.

(23) Ploetz, E.; Marx, B.; Klein, T.; Huber, R.; Gilch, P. *Optics Express* **2009**, *17*, 18612–18620.

(24) Ye, T.; Fu, D.; Warren, W. S. *Photochem. Photobiol.* **2009**, *85*, 631–645.

(25) Vartiainen, E. M.; Rinia, H. A.; Muller, M.; Bonn, M. *Optics Express* **2006**, *14*, 3622–3630.

(26) Shen, Y. R. *The Principles of Nonlinear Optics*; Wiley Interscience: New York, 1984.

(27) Rinia, H. A.; Bonn, M.; Muller, M.; Vartiainen, E. M. *ChemPhysChem* **2007**, *8*, 279–287.

(28) Zimmerley, M.; McClure, R. A.; Choi, B.; Potma, E. O. *Appl. Opt.* **2009**, *48*, D79–87.

(29) Zimmerley, M.; Lin, C.-Y.; Oertel, D. C.; Marsh, J. M.; Ward, J. L.; Potma, E. O. *J. Biomed. Optics* **2009**, *14*, 044019.

(30) Bergner, G.; Chatzipapadopoulos, S.; Akimov, D.; Dietzek, B.; Malsch, D.; Henkel, T.; Schlucker, S.; Popp, J. *Small* **2009**, *5*, 2816–2818.

(31) Heinrich, C.; Hofer, A.; Ritsch, A.; Ciardi, C.; Bernet, S.; Ritsch-Marte, M. *Optics Express* **2008**, *16*, 2699–2708.

(32) Li, L.; Wang, H.; Cheng, J.-X. *Biophys. J.* **2005**, *89*, 3480–3490.

(33) Ganikhanov, F.; Evans, C. L.; Saar, B. G.; Xie, X. S. *Opt. Lett.* **2006**, *31*, 1872–1874.

(34) Chen, B.-C.; Sung, J.; Lim, S. H. *J. Phys. Chem. B* **2010**, *114*, 16871–16880.

(35) Lee, Y. J.; Parekh, S. H.; Kim, Y. H.; Cicerone, M. T. *Optics Express* **2010**, *18*, 4371–4379.

(36) Volkmer, A.; Book, L. D.; Xie, X. S. *Appl. Phys. Lett.* **2002**, *80*, 1505–1507.

(37) von Vacano, B.; Motzkus, M. *Phys. Chem. Chem. Phys.* **2008**, *10*, 681–691.

(38) Cheng, J.-X.; Volkmer, A.; Book, L. D.; Xie, X. S. *J. Phys. Chem. B* **2002**, *106*, 8493–8498.

(39) Muller, M.; Schins, J. M. *J. Phys. Chem. B* **2002**, *106*, 3715–3723.

(40) Wurpel, G. W. H.; Schins, J. M.; Muller, M. *J. Phys. Chem. B* **2004**, *108*, 3400–3403.

(41) Rinia, H. A.; Bonn, M.; Muller, M. *J. Phys. Chem. B* **2006**, *110*, 4472–4479.

(42) von Vacano, B.; Meyer, L.; Motzkus, M. *J. Raman Spectrosc.* **2007**, *38*, 916–926.

(43) Wurpel, G. W. H.; Muller, M. *Chem. Phys. Lett.* **2006**, *425*, 336–341.

(44) Evans, C. L.; Potma, E. O.; Xie, X. S. *Opt. Lett.* **2004**, *29*, 2923–2925.

(45) Potma, E. O.; Evans, C. L.; Xie, X. S. *Opt. Lett.* **2006**, *31*, 241–243.

(46) Jurna, M.; Korterik, J. P.; Otto, C.; Herek, J. L.; Offerhaus, H. L. *Optics Express* **2008**, *16*, 15863–15869.

(47) von Vacano, B.; Buckup, T.; Motzkus, M. *Opt. Lett.* **2006**, *31*, 2495–2497.

(48) Chowdary, P. D.; Benalcazar, W. A.; Jiang, Z.; Marks, D. L.; Boppart, S. A.; Gruebele, M. *Anal. Chem.* **2010**, *82*, 3812–3818.

(49) Jurna, M.; Garbacik, E. T.; Korterik, J. P.; Herek, J. L.; Otto, C.; Offerhaus, H. L. *Anal. Chem.* **2010**, *82*, 7656–7659.

(50) Millane, R. P. *J. Opt. Soc. Am. A* **1990**, *7*, 394–411.

(51) Vartiainen, E. M.; Peiponen, K.-E.; Asakura, T. *Appl. Spectrosc.* **1996**, *50*, 1283–1289.

(52) Liu, Y.; Lee, Y. J.; Cicerone, M. T. *Opt. Lett.* **2009**, *34*, 1363–1365.

(53) Sung, J.; Chen, B.-C.; Lim, S.-H. *J. Raman Spectrosc.* **2010**In press.

(54) Parekh, S. H.; Lee, Y. J.; Aamer, K. A.; Cicerone, M. T. *Biophys. J.* **2010**, *99*, 2695–2704.

(55) Vartiainen, E. M. *J. Opt. Soc. Am. B* **1992**, *9*, 1209–1214.

(56) Petrov, G. I.; Arora, R.; Yakovlev, V. V.; Wang, X.; Sokolov, A. V.; Scully, M. O. *Proc. Natl. Acad. Sci. U.S.A.* **2007**, *104*, 7776–7779.

(57) Liu, Y.; Lee, Y. J.; Cicerone, M. T. *J. Raman Spectrosc.* **2008**, *40*, 726–731.

(58) de Juan, A.; Maeder, M.; Hancewicz, T.; Duponchel, L.; Tauler, R. Chemometric Tools for Image Analysis In *Infrared and Raman Spectroscopic Imaging*; Salzer, R., Siesler, H. W., Eds.; Wiley-VCH: Weinheim, Germany, 2009.

(59) Bro, R.; de Jong, S. *J. Chemometrics* **1997**, *22*, 393–401.

(60) Okuno, M.; Kano, H.; Leproux, P.; Couderc, V.; Day, J. P. R.; Bonn, M.; Hamaguchi, H. *Angew. Chem., Int. Ed.* **2010**, *49*, 6773–6777.

(61) Malinowski, E. R. *Factor Analysis in Chemistry*, 3rd ed.; Wiley Interscience: New York, 2002.

(62) Widjaja, E.; Crane, N.; Chen, T.-C.; Morris, M. D.; Ignelzi, M. A.; McCreadie, B. R. *Appl. Spectrosc.* **2003**, *57*, 1353–1362.

(63) Lasch, P.; Haensch, W.; Diem, M. *Biochim. Biophys. Acta* **2004**, *1688*, 176–186.

L

dx.doi.org/10.1021/jp200606e |*J. Phys. Chem. B* XXXX, XXX, 000–000

(64) Schafer, D.; Muller, M.; Bonn, M.; Marr, D. W. M.; van Maarseveen, J.; Squier, J. A. *Opt. Lett.* **2009**, *34*, 211–213.

(65) Day, J. P. R.; Rago, G.; Domke, K. F.; Velikov, K. P.; Bonn, M. *J. Am. Chem. Soc.* **2010**, *132*, 8433–8439.

(66) Rinia, H. A.; Burger, K. N. J.; Bonn, M.; Muller, M. *Biophys. J.* **2008**, *95*, 4908–4914.

(67) Min, W.; Lu, S.; Holtom, G. R.; Xie, X. S. *ChemPhysChem* **2009**, *10*, 344–347.